Unified description of nuclear stopping in central heavy-ion collisions from 10*A* MeV to 1.2*A* GeV

G. Q. Zhang,[1,2] Y. G. Ma,[1,*] X. G. Cao,[1] C. L. Zhou,[1,2] X. Z. Cai,[1] D. Q. Fang,[1] W. D. Tian,[1] and H. W. Wang[1]

[1]*Shanghai Institute of Applied Physics, Chinese Academy of Sciences, Shanghai 201800, China*

[2]*Graduate School of the Chinese Academy of Sciences, Beijing 100080, China*

(Received 24 November 2010; revised manuscript received 25 July 2011; published 26 September 2011)

A detailed analysis of the wide excitation function of nuclear stopping has been conducted within a transport model, isospin-dependent quantum molecular dynamics model, and an overall good agreement with the INDRA and FOPI Collaborations' experimental data has been achieved. It is found that the mean value of isotropy in central heavy-ion collision (HIC) reaches a minimum near-Fermi energy and approaches a maximum at around 300–400*A* MeV. This suggests that, in statistical average, the equilibration is far from being reached, even in central HIC especially near Fermi energy. A hierarchy in the stopping of fragments, which favors heavy fragments to penetrate, provides a robust restriction on the global trend of nuclear stopping and could serve as a probe for nuclear equations of state.

DOI: 10.1103/PhysRevC.84.034612 PACS number(s): 25.70.−z, 21.65.Mn

I. INTRODUCTION

The equation of state (EOS) of nuclear matter and its transport mechanisms are the focus of heavy-ion collisions (HICs) during the past three decades [1–8]. Before the early 1980s, hydrodynamics approaches based on the local equilibration postulate were provided to extract the EOS information from experimental observables [9]. The discovery of collective flow seems to confirm these approaches and their corresponding equilibration conditions. With the development of microscopic transport theories, it is found that the local equilibration postulate is not indispensable. Actually, near Fermi energy, both statistical and dynamical models which are based on very different, even contradictory mechanisms can predict the same multifragmentation phenomenon [10].

During the central HIC process, nuclear stopping governs most of the dissipated energy and constrains the different reaction mechanisms at different incident energies. It can provide information on the EOS, nucleon-nucleon (N-N) cross section, and the degree of equilibrium reached in HIC [11–20]. Recently, the INDRA and ALADIN Collaborations investigated event-by-event nuclear stopping in central HICs at intermediate energies by a 4π multidetector [12]. In the experiment [12] a striking minimal stopping at 40*A* MeV (Fermi energy) for a Xe + Sn system was observed. These experimental results have the potential to provide important information about the properties of the nuclear matter and to discover critical clues for the entire dynamical process during HIC. In a previous comparison between experimental results and an isospin-dependent quantum molecular dynamics model (IQMD) simulation [13], a significant difference between them was observed. In the experiment [12], below 70*A* MeV the authors show experimental data far below the IQMD simulation results and argue that the IQMD model overpredicts nuclear stopping power at low energy. However, before comparing the experimental results quantitatively with those of the transport model, two important ingredients should be carefully considered. One is the difference between nucleon phase space (the momentum and positions ensemble of all nucleons) and fragment phase space (the momentum and positions ensemble of all fragments) in IQMD, and the other is the criterion of centrality in the experiment. After these two elements are factored in, we find that the nuclear stopping could serve as a potential probe for determining the nuclear EOS.

This article is organized as follows: After introducing some details on the IQMD model in Sec. II, two relevant factors are reconsidered in Sec. III: one is the difference between nucleon phase space and fragment phase space, and the other is the mixing of impact parameter. Then we compare the simulation results of IQMD with the INDRA Collaboration's experiments near Fermi energy as well as the FOPI Collaboration's at higher energy in Sec. IV. A summary and conclusions are given in Sec. V.

II. ISOSPIN-DEPENDENT QUANTUM MOLECULAR DYNAMICS MODEL

The quantum molecular dynamics (QMD) [21] model is an *n*-body theory to predict the behavior of HIC at intermediate energies on an event-by-event basis. The IQMD [22,23] model, as inherited from the QMD model, considers various aspects of the isospin effects: the differing density distributions for neutrons and protons, the asymmetry potential term in a mean field, the experimental cross section for nucleon-nucleon interaction ($\sigma_{np} \approx 3\sigma_{pp}, \sigma_{pp} = \sigma_{nn}$), and Pauli blocking for neutrons and protons separately. As in QMD, each nucleon wave function is represented as a Gaussian form in IQMD, which is defined as

$$\phi_i(\vec{r}, t) = \frac{1}{(2\pi L)^{3/4}} \exp\left(-\frac{[\vec{r} - \vec{r}_i(t)]^2}{4L}\right) \exp\left(-\frac{i\vec{r} \cdot \vec{p}_i(t)}{\hbar}\right). \quad (1)$$

Here L is the width parameter for the Gaussian wave packet, which is found to be dependent on the size of the reacting system, to constrain the stability of the system. We use $L = 2.16$ fm^2 for the Xe + Sn system. The $\vec{r}_i(t)$ and $\vec{p}_i(t)$

*Author to whom all correspondence should be addressed: ygma@sinap.ac.cn

are the position and momentum coordinates of the nucleon. By performing the variation method, equations of the time evolution of the mean position $\vec{r}_i(t)$ and momentum $\vec{p}_i(t)$ are found to be well-known Hamilton equations of motion,

$$\dot{\vec{p}}_i = -\frac{\partial\langle H\rangle}{\partial\vec{r}_i} \quad \text{and} \quad \dot{\vec{r}}_i = \frac{\partial\langle H\rangle}{\partial\vec{p}_i}, \tag{2}$$

where $\langle H\rangle$ is the Hamiltonian of the system. So now the problem is to calculate the Hamiltonian of the system.

After applying the Wigner transformation to the single-nucleon wave function, one can get the Wigner distribution function to describe a single nucleon density in phase space, defined as

$$f_i(\vec{r},\vec{p},t) = \frac{1}{\pi^3\hbar^3} e^{-[\vec{r}-\vec{r}_i(t)]^2\frac{1}{2L}} e^{-[\vec{p}-\vec{p}_i(t)]^2\frac{2L}{\hbar^2}}, \tag{3}$$

and the total density of the system is the sum over all the nucleons.

Then we can get the total Hamiltonian in the IQMD model

$$\langle H\rangle = \langle T\rangle + \langle V\rangle, \tag{4}$$

where the mean-field part is

$$\langle V\rangle = \frac{1}{2}\sum_i\sum_{j\neq i}\int f_i(\vec{r},\vec{p},t) \times V^{ij} f_j(\vec{r}\,',\vec{p}\,',t)\,d\vec{r}\,d\vec{r}\,'d\vec{p}\,d\vec{p}\,'. \tag{5}$$

In the QMD model, the two-body potential interaction contains the Coulomb interaction and the real part of the G matrix. The later one can be divided into three parts: the contact Skyrme-type interaction, a finite-range Yukawa potential, and a momentum-dependent interaction (subscript mdi) part. Mathematically, the two-body potential interaction can be written as

$$\begin{aligned} V^{ij} &= G^{ij} + V^{ij}_{\text{Coul}} \\ &= V^{ij}_{\text{Skyrme}} + V^{ij}_{\text{Yuk}} + V^{ij}_{\text{mdi}} + V^{ij}_{\text{Coul}} \\ &= t_1\delta(\vec{x}_i-\vec{x}_j) + t_2\delta(\vec{x}_i-\vec{x}_j)\rho^{\gamma-1}(\vec{x}_i) \\ &\quad + t_3\frac{\exp\{-|\vec{x}_i-\vec{x}_j|/\mu\}}{|\vec{x}_i-\vec{x}_j|/\mu} \\ &\quad + t_4\ln^2[1+t_5(\vec{p}_i-\vec{p}_j)^2]\delta(\vec{x}_i-\vec{x}_j) + \frac{Z_iZ_je^2}{|\vec{x}_i-\vec{x}_j|}, \end{aligned} \tag{6}$$

where Z is the charge of the baryon, and $t_1 \ldots t_5$ and μ are the parameters to fit the real part of the G matrix and the properties of nuclei. For the IQMD model, one additional part, the symmetry potential V^{ij}_{sym}, is added to take into account the isospin effects. The total potential in IQMD is then written as

$$V^{ij} = V^{ij}_{\text{Skyrme}} + V^{ij}_{\text{Yuk}} + V^{ij}_{\text{mdi}} + V^{ij}_{\text{Coul}} + V^{ij}_{\text{sym}}, \tag{7}$$

where the symmetry potential is

$$V^{ij}_{\text{sym}} = t_6\frac{1}{\rho_0}T_{3i}T_{3j}\delta(\vec{r}_i-\vec{r}_j), \tag{8}$$

with $t_6 = 100$ MeV for fitting the Bethe-Weizsäcker mass formula, T_3 is the isospin third projection, and ρ_0 is the nuclear saturation density (0.16 fm^{-3}).

We focus on the Skyrme potential and the momentum-dependent potential, due to their special connection to nuclear EOS.

One can fulfill the calculation for the Skyrme potential and momentum dependence in Eq. (5) by introducing the interaction density,

$$\rho^i_{\text{int}}(\vec{r}_i) = \frac{1}{(4\pi L)^{3/2}}\sum_{j\neq i} e^{-(\vec{r}_i-\vec{r}_j)^2/(4L)}. \tag{9}$$

The momentum-dependent potential, which may be optional in QMD and IQMD, is parameterized with the experimental data and can be written as

$$U_{\text{mdi}} = \delta\ln^2[\epsilon\,(\Delta\vec{p})^2+1]\left(\frac{\rho_{\text{int}}}{\rho_0}\right), \tag{10}$$

where $\delta = 1.57$ MeV and $\epsilon = 500$ (GeV/c)$^{-2}$ are taken from the measured energy dependence of the proton-nucleus optical potential [24] and $\rho_{\text{int}} = \sum\rho^i_{\text{int}}(\vec{r}_i)$.

The Skyrme potential is

$$U^{\text{Skyrme}} = \alpha\left[\frac{\rho_{\text{int}}}{\rho_0}\right] + \beta\left[\frac{\rho_{\text{int}}}{\rho_0}\right]^\gamma, \tag{11}$$

where α, β, and γ are the Skyrme parameters, which connect tightly with the EOS of bulk nuclear matter. After fitting the minimum binding energy and the compressibility at the saturation density, one can get the parameters. The nuclear compressibility, which is the second derivative of the energy at the minimum with respect to the density, is expressed as

$$\kappa = 9\rho^2\frac{\partial^2}{\partial\rho^2}\left(\frac{E}{A}\right), \tag{12}$$

where $\kappa = 200$ MeV means soft EOS, while $\kappa = 380$ MeV is for hard EOS. See Table I for the Skyrme sets of parameters for different EOS.

The other terms can be also calculated by applying the convolution of the interaction with the Wigner distribution function. After all the potential terms are determined, one can solve the equations of motion of the baryons. For the mesons, only Coulomb force is considered.

For the collisions, IQMD uses the experimental cross section which shows the isospin effects and nuclear medium effect [22]. To consider the fermion property, Pauli blocking is also adopted after the collisions.

IQMD treats the many-body state explicitly, contains correlation effects to all orders, and deals with fragmentation

TABLE I. Parameter sets for the nuclear equation of state used in the QMD model. S and H refer to the soft (compressibility κ =200 MeV) and hard equations of state (compressibility κ = 380 MeV), and M refers to the inclusion of momentum-dependent interaction. The results are taken from [22].

	α (MeV)	β (MeV)	γ	δ (MeV)	$\varepsilon\left(\frac{c^2}{\text{GeV}^2}\right)$
S	−356	303	1.17	—	—
SM	−390	320	1.14	1.57	500
H	−124	71	2.00	—	—
HM	−130	59	2.09	1.57	500

and fluctuation of HICs naturally. To recognize fragments produced in HICs, a simple coalescence rule is used with the criteria $\Delta r = 3.5$ fm and $\Delta p = 300$ MeV/c between two considered nucleons. Thus, nucleons dominated in Fermi motion will be constrained in the fragments.

III. DIFFERENCE BETWEEN NUCLEON PHASE SPACE AND FRAGMENT PHASE SPACE AND IMPACT PARAMETER MIXING

To describe nuclear stopping power, the ratio of transverse to parallel quantities is used in the experiment [12]. One definition is the energy-based isotropy ratio R_E,

$$R_E = \frac{\sum E_{ti}}{2\sum E_{li}}, \tag{13}$$

where $E_{ti}(E_{li})$ is the transverse (parallel) kinetic energy in center of mass system (c.m.) the sum runs over all products event by event. One can expect $R_E = 1$ for isotropy or full stopping, $R_E < 1$ for partial transparency, and $R_E > 1$ for superstopping. Another definition is R_p,

$$R_p = \frac{2\sum |p_{ti}|}{\pi \sum |p_{li}|}, \tag{14}$$

where momenta are used instead of energies. However, they are actually the different forms of physics realization of the classical Maxwell distribution assumption.

At low energy, two-body collision between nucleons is greatly suppressed by Pauli blocking and the mean field governs the HIC process. At the freeze-out stage, the motion of a large portion of nucleons is limited in certain fragments, in which Fermi motion dominates over the others, while at higher energy, two-body collision plays the dominant role and most of the nucleons suffer violent collisions and get excited to become free. In this case, the fragment phase space tends to get closer to the nucleon phase space. In previous IQMD simulation by Liu *et al.* [13], the nuclear stopping was investigated from nucleon phase space at intermediate energy, where the isotropic Fermi motion still plays a large role. In comparison with the experimental data of the stopping, the fragment phase space should be applied at intermediate energy within the IQMD model rather than nucleon phase space.

In Fig. 1 we show the results of stopping, defined as the ratio of transverse momenta to parallel momenta R_p, in nucleon phase space and fragment phase space, respectively. The scaled impact parameter $b_{\rm red} < 0.1$ ($b_{\rm red} = b/b_{\rm max}$) is adopted, with $b_{\rm max} = 1.12(A_P^{1/3} + A_T^{1/3})$ fm, where A_P and A_T are the mass of projectile and target, respectively. Apparently, stopping calculated in nucleon phase space almost reaches the saturated value, just like Liu's situation [13]. While in the case of fragment phase space, stopping is far below the saturated value and gets closer to the experimental value. This underlies that, at low incident energy, nuclear stopping obtained from fragment phase space is more sensitive as compared to the nucleon phase space and tends to fill the gap between theory and experimentation. At higher incident energy (above 100A MeV), the difference between stopping presented in nucleon phase space and fragment space in IQMD

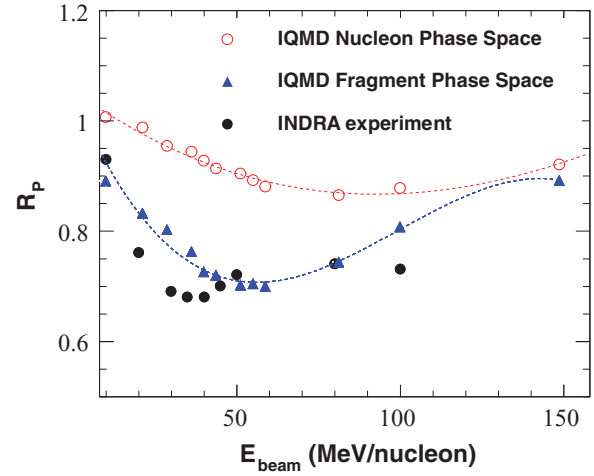

FIG. 1. (Color online) Comparison between experimental stopping values [12] (black points) and predictions of IQMD calculation in nucleon phase space (red open circles) and fragment phase space (blue up triangles) for central ^{129}Xe + ^{120}Sn collision. The two lines are for guiding the eyes. IQMD adopts the hard EOS and $b_{\rm red} < 0.1$.

tends to be smaller. However, a minimum stopping with value 0.70 at about 55A MeV is shown in IQMD, compared with a value of 0.68 at 40A MeV in experiments. This difference may come from the different criteria of centrality between the IQMD and experiment.

To avoid autocorrelations, total charged particle multiplicity ($N_{\rm ch}$) in the experiment [12] is chosen as the criterion of the centrality. However, the largest $N_{\rm ch}$ does not mean the highest centrality, due to event-by-event fluctuation. On one hand, $N_{\rm ch}$ gets saturated at a certain centrality and then central and near-central HIC provide similar $N_{\rm ch}$ values. On the other hand, due to the dynamical fluctuation, $N_{\rm ch}$ at certain centralities presents a broad distribution. Thus, the HIC at different centralities may very likely share the same $N_{\rm ch}$. Hence if $N_{\rm ch}$ is adopted for the criterion of the centrality, it is expected that the impact parameters will suffer a great mixing and cover a wide range, which will decrease the stopping power and increase the fluctuation of the HIC system greatly.

We now use the IQMD model to elucidate the impact parameter mixing situation. In the experiment [12], a typical cross section of 50 mb for the most total charged particle multiplicity is taken for all HIC systems. Within the IQMD model, we calculate the mean $N_{\rm ch}$ and its width at head-on collision ($b_{\rm red} = 0$). Then a low limit is set as the mean $N_{\rm ch}$ with its half-width off. In Fig. 2(a), the IQMD model reproduces well the experimental results of the INDRA and ALADIN Collaborations [12], except giving a little higher $N_{\rm ch}$. (Note that the experimental filter is not used in the present calculation.) The red dashed line at $N_{\rm ch} = 44$ is the low limit for central collision in the IQMD, which is comparable with $N_{\rm ch} = 36$ in the experiment. In Fig. 2(b), a mean value of stopping (R_E) at around $0.6 - 0.7$ is observed in the exact central collision, which has a decreasing trend with the increase of impact parameter. When the cut $N_{\rm ch} = 44$ is applied, there is a broad distribution of impact parameter in Fig. 2(d), and a lower mean value of stopping at about 0.56 with a width

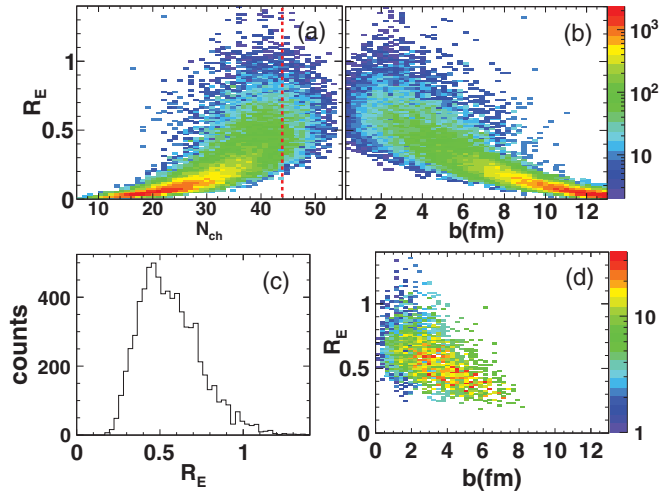

FIG. 2. (Color online) IQMD simulation with the hard EOS for ^{129}Xe + ^{119}Sn collisions at 50A MeV. (a) Bidimensional correlation plot between the mean value of stopping and the total charged particle multiplicity, same as Fig. 1(b) in Ref. [12]. (b) Bidimensional correlation plot between the mean value of stopping and impact parameter. (c) Distribution of R_E for central collisions. (d) Same as (b), but with central collision cut.

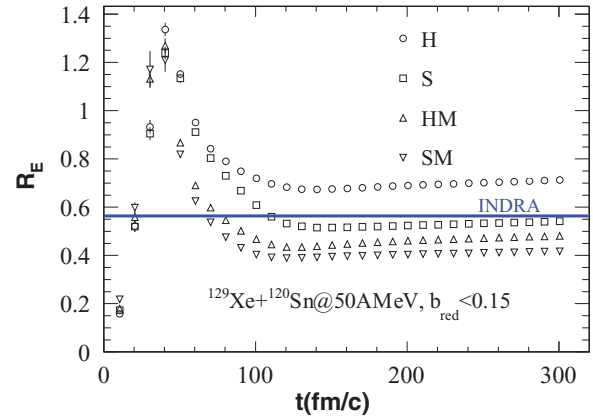

FIG. 3. (Color online) Energy-based stopping values evolution with time for ^{129}Xe + ^{120}Sn at 50A MeV and $b_{\rm red} < 0.15$ in IQMD (open symbols) and experimental data (solid line) [12]. Circles, squares, up-triangles, and down-triangles represent our calculations with the hard (H), the soft (S), the hard with MDI (HM), and the soft with MDI (SM) for EOS, respectively. The horizontal line represents the measured result by the INDRA Collaboration (not for the time evolution).

of about 0.42 in Fig. 2(c), which is comparable with a mean value of 0.56 with a width of 0.47 in the experiment [12]. In this context, a better criterion of centrality should be provided to reduce the probability of impact parameter mixing at low energies.

IV. RESULTS AND DISCUSSION

Taking the above two key ingredients into account, we can compare the experimental results with those of the IQMD quantitatively. To have a broad view of the nuclear stopping, a systematic simulation of ^{129}Xe + ^{120}Sn is made in very central HIC ($b_{\rm red} < 0.15$) from 10A MeV to 1.2A GeV to cover most of the intermediate energy range, where our results can be compared with the recent INDRA and FOPI data [11,17].

It should be noted that related but different definitions of stopping are adopted by the INDRA [12] and FOPI [11,17,19] Collaborations, respectively. The event-by-event stopping (event level), defined as the ratio of transverse to parallel kinetic energies, was adopted by the INDRA and ALADIN Collaborations (i.e., R_E). The ratio of the variances of the transverse to those of the longitudinal rapidity distribution of fragments (fragment level) is taken in the case of the FOPI experiment:

$$vartl = \frac{(\Delta y_t)^2}{(\Delta y_l)^2}. \qquad (15)$$

Despite this, they both still show the global stopping power of central HIC. When a full stopping stage (likely to be in equilibration) is reached, both R_E and $vartl$ are required with a unit value.

Now we compare our results with the INDRA experiment. The central ($b_{\rm red} < 0.15$) collision of ^{129}Xe +^{120}Sn, at incident energy 50A MeV, is taken as an example. The time evolution of the stopping (defined in R_E) for various EOS are shown in Fig. 3. The stopping for different EOS presents the same trend. The stopping rises at the early compression stage, drops down at the following expansion stage, and becomes stable after the system reaches the freeze-out. This is consistent with the results from works of [13] and [14], which are in nucleon phase space. However, the stopping power shows EOS dependence. The hard EOS shows higher stopping than the soft EOS, during the whole time evolution. This is because the hard EOS nuclear matter is harder to compress than the soft one. When compressed from the longitudinal direction, the hard EOS nuclear matter will squeeze out more than the soft one through transverse expansion. The momentum-dependent force decreases the stopping power of the system, which may result from its repulsive nature and an increase in the mean-free path [24]. At this incident energy, the INDRA experimental result seems to support the soft EOS.

Here the time adopted in IQMD for the freeze-out stage is 200 fm/c. For the case of low incident energy, the heavy fragments may still stay at an excited state, which would the de-excite themselves by emissing free nucleons, light charged particle (LCP), and γ rays at the later stage. Based on this consideration, some hybrid models, a dynamical one followed by a statistical one, come into the play, such as AMD + GEMINI [25–27] and HIPSE + SIMON [28], etc. They do fit the experimental fragment distribution very well. At the same time, the de-excitation procedure may also extend both the transverse and longitudinal width of rapidity of the final fragments, which smears the original stopping at the fragment level. Especially, the big fragments at high excitation stages will also emit free nucleons or LCPs, which will increase the isotropy of the system. This might be very serious for the lower-energy ($\leqslant$40A MeV) case because more heavy fragments are left. As a compensation, the freeze-out time is delayed from 200 to 300 fm/c (or even later), but no great

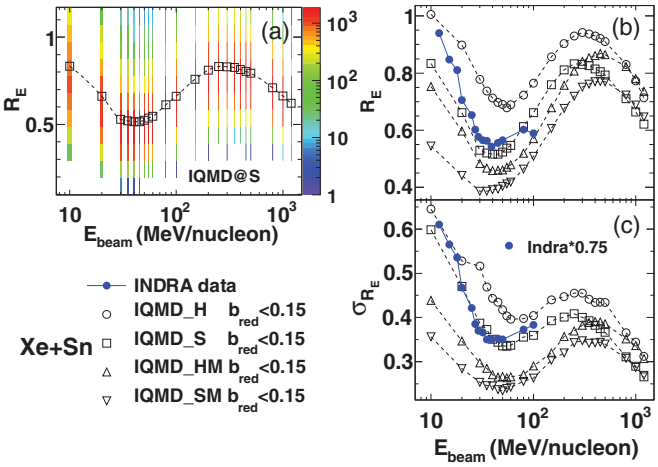

FIG. 4. (Color online) Stopping and its width as a function of incident energy with different EOS for central ^{129}Xe + ^{120}Sn collision in IQMD (open symbols) and experimental data (solid circles) [12]. (a) Bidimensional plots show the distribution of R_E. (b) The mean value of stopping. (c) The width of stopping. (Note the widths of experiment have been scaled by a factor of 0.75.) Circles, squares, up-triangles, and down-triangles represent our calculations with the hard (H), the soft (S), the hard with MDI (HM), and the soft with MDI (SM) for EOS, respectively.

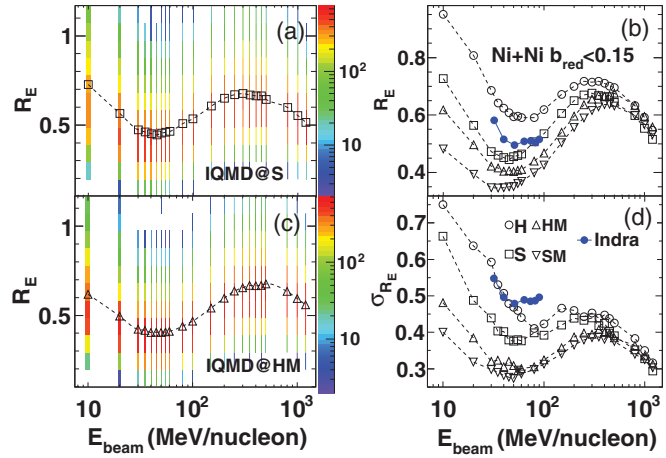

FIG. 5. (Color online) Same as Fig. 4, but for the ^{58}Ni + ^{58}Ni system. One more case (HM) is added in (c) to see the distribution of R_E.

changes happen, except the intermediate mass fragment (IMF) raises their stopping values a little higher. For higher energy ($\geqslant 100A$ MeV), since very few heavy fragments exist, it is not necessary to evolute the system with such a long time or de-excite the system with a statistical process [29].

Figure 4 shows the excitation function of the mean value of R_E and its width σ_{R_E} for ^{129}Xe +^{120}Sn by using different EOSs. In Fig. 4(a), the soft EOS with the compressibility of $\kappa = 200$ MeV is taken to show the distribution of R_E with incident energies. In Figs. 4(b) and 4(c), the mean R_E and its width σ_{R_E} show the same trends, consistent with the experimental results [12]. Scaled by 0.75, the width of stopping in the experiment of INDRA is compared with the simulation results. The broader widths in experiment could come from the impact parameter mixing, as we have discussed in Sec. II. For all of the considered energy range, the hard EOS with $\kappa = 380$ MeV shows stronger stopping than the soft EOS. The EOS with momentum-dependent interaction (MDI) [24] tends to decrease the stopping at energy below $500A$ MeV. While the weight of MDI tends to vanish above $500A$ MeV. Near the Fermi energy, we also observe a minimum of stopping with its minimal width for all EOS. The EOS with MDI favors more penetration and consumes less energy to reach the minimal stopping. The present experimental results seem to favor the soft EOS around Fermi energy. This is consistent with recent conclusions on the soft hadronic matter based on Kaon spectral analysis at higher energy [6,7]. At $300 - 400A$ MeV, a maximum of stopping accompanied by its maximal width is seen for all EOSs. This is comparable to the recent experimental results of the FOPI Collaboration [11,17,19].

The smaller size collision system ^{58}Ni + ^{58}Ni is also investigated to see the stopping behavior, and similar behaviors are found in comparison with the case of ^{129}Xe + ^{120}Sn, except that ^{58}Ni + ^{58}Ni shows lower stopping power. Again, note that the INDRA data seems to support the soft EOS case [Fig. 5(b)].

Figure 6(a) displays the atomic number (Z) hierarchy of the degree of stopping at different fragment levels and different incident energies. From small fragment $Z = 1$ with stopping value $0.7 - 0.9$ to an intermediate one $Z = 10$ with $0.1 - 0.2$, it is seen that the stopping power drops quickly as Z of the fragment increases. A similar trend has been experimentally observed Au + Au, Xe + CsI, and Ni + Ni central collisions at $150A$ MeV, $250A$ MeV, and $400A$ MeV by the FOPI Collaboration [11,19,30].

The hierarchies also show the incident energy dependence. On the one hand, at $300A$ MeV [open diamond in Fig. 6(a)]

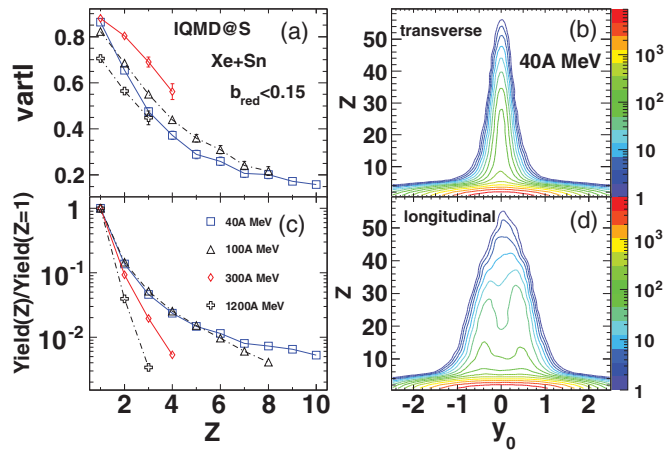

FIG. 6. (Color online) Stopping hierarchy in IQMD with the soft EOS for central ^{129}Xe + ^{120}Sn collision. Four energy points, namely, 40, 100, 300, and $1200A$ MeV, are investigated. (a, c) Z-dependent stopping at the fragment level and the yield of fragments (scaled by $Z = 1$), respectively. (b, d) Bidimensional distributions of transverse and longitudinal rapidity for different fragments at $40A$ MeV, respectively.

the fragments show stronger stopping than those at the others, which is consistent with the maximum event-level stopping at the same energies in Fig. 4. This may suggest a state close to equilibration. On the other hand, at 40A MeV [open square in Fig. 6(a)] where the stopping at event level reaches a minimum [Fig. 4(b)], the stopping at fragment level does show its corresponding smallest value. At this incident energy, most of the nucleons are confined in certain fragments, which also reduces the stopping value at the event level. Near Fermi energy, the relative yields of intermediate-mass fragments (scaled by $Z = 1$) are higher than those at the others, as shown in Fig. 6(c), which will lead to the smallest effective power-law exponents in charge distribution [31]. For a further understanding of the minimal stopping near Fermi energy, Figs. 6(b) and 6(d) present a holographic two-dimensional (2D) histogram of transverse and longitudinal rapidity for different charge of fragments (rapidity has been scaled by the projectile rapidity in the center-of-mass system). From $Z = 1$ to larger Z, the longitudinal rapidity distributions become relatively broader than the transverse rapidity distributions. In addition, for those fragments with Z larger than about 4, two clear peaks in the longitudinal rapidity stand prominently, corresponding to projectilelike and targetlike contributions. This means at Fermi energy, equilibration is far from being reached and entrance channel effects remain strong even in central HIC, while at high energy 1.2A-GeV fragments are the most transparent.

It is highly expected that the hierarchy would help to determine nuclear EOS. Figure 7 shows Z-dependent stopping for four different energies with different EOS in IQMD. The hard EOS case shows higher stopping at the fragment level than the soft EOS case, and the MDI always makes it easy for the fragments to penetrate. At lower energy [150A MeV in Fig. 7(b)], the EOS without MDI agrees with FOPI data [11] much better (Xe + CsI are similar system as Xe + Sn). On the contrary, at higher energies [Figs. 7(c) and 7(d)] in order to reproduce experimental data, the weight of MDI should be increased. More information could be extracted once more experimental data are provided to lower the statistical fluctuation. In addition, at energy near Fermi energy, as shown in Fig. 7(a), it would be worthwhile to perform experiments to obtain Z-dependent stopping, which is important to understanding the minimal stopping at the event level at Fermi energy as well as to constrain the EOS.

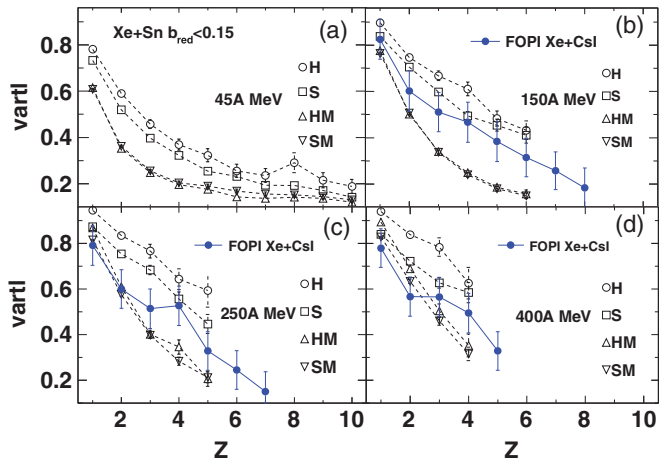

FIG. 7. (Color online) Atomic number dependence of the stopping observable *vartl* for fragments emitted in central ^{129}Xe + ^{120}Sn collisions. Open symbols represent our calculations with different EOS and solid symbols with error bar denote the available experimental data [11]. (a) 45A MeV (no experimental data available yet); (b) 150A MeV; (c) 250A MeV; and (d) 400A MeV.

The observable dependence of stopping on atomic number suggests that the heavier fragments have less stopping. This indicates that the heavier fragments are more transparent and keep a stronger entrance channel memory even in the central nuclear collision. This supports the argument that the fragments are not formed in a globally equilibrated environment [21], which contradicts the assumption of equilibrium required by ideal fluid hydrodynamics. A self-consistent explanation is provided in [19]: if a heavier fragment can survive during the process of HIC, its constituent nucleons should have suffered a less violent collision history. Based on this consideration, the stopping hierarchy at the fragment level would also reflect the N-N cross section. This explanation is also quantitatively demonstrated in earlier versions of QMD [32]. Another explanation is due to the corona effect (geometrical) [33], even in very central collisions in which those nucleons near the surface of a projectile or target would suffer less collision history than those inside. Thus, they would keep their original direction and compose the final heavy residues.

In very central HIC, the incident energy dependence of stopping can be understood in a unified structure based on Pauli blocking, mean-field, and N-N collision. At intermediate energy, two-body collisions between nucleons always increases the dissipation of the HIC system and tends to favor more isotropy, while Pauli blocking suppresses N-N collision at low energy and the mean field forms collective motion. This picture shows incident energy dependence. Below Fermi energy, the HIC system has enough time to reach an equilibration state because of the slow process of the reaction. Near Fermi energy, N-N collision is greatly suppressed by Pauli blocking and nucleons tend to keep their original moving state and have an entrance effect. Meanwhile, the mean field dominates HIC and clusters are then favored. Above Fermi energy, two-body collisions between nucleons come to play the dominant role and reach their maximal effect at 300 − 400A MeV. At higher energy, the mean-free path of the nucleon increases because of the smaller N-N cross section; thus most of the nucleons will pass through each other.

V. SUMMARY AND CONCLUSIONS

In summary, we successfully describe the wide-range excitation function of nuclear stopping from 10A MeV to 1.2A GeV with a transport model IQMD. A minimum of nuclear stopping value near Fermi energy and a maximum at about 300A MeV in very central HIC matches the INDRA and FOPI data very well. The former indicates that in statistical average, the equilibration state is far from being reached near Fermi energy, even in very central HIC. Meanwhile, the hierarchy of stopping observable together with the yields of

fragments provides us a decomposition way to understand the whole stopping excitation function. Around Fermi energy, the soft EOS seems the best, while at energy from 250 to 400*A* MeV, the role of MDI becomes important. In addition, it is also highly expected that the isospin, which has been regarded to reach its equilibration the fastest at the early HIC process, might also get a great penetration in very central HIC near Fermi energy.

ACKNOWLEDGMENTS

This work is partially supported by the NSFC under Contract Nos. 11035009, 10979074, 10875160, 10805067, and 10975174, the 973-Program under Contract No. 2007CB815004, the Shanghai Development Foundation for Science and Technology under Contract No. 09JC1416800, and the Knowledge Innovation Project of the Chinese Academy of Sciences under Grant No. KJCX2-EW-N01.

[1] P. Danielewicz, R. Lacey, and W. G. Lynch, Science **298**, 1592 (2002).
[2] B. A. Li, L. W. Chen and C. M. Ko, Phys. Rep. **464**, 113 (2008).
[3] V. Baran, M. Colonna, V. Greco, and M. Di Toro, Phys. Rep. **410**, 335 (2005).
[4] M. B. Tsang, Y. Zhang, P. Danielewicz, M. Famiano, Z. Li, W. G. Lynch, and A. W. Steiner, Phys. Rev. Lett. **102**, 122701 (2009).
[5] J. B. Natowitz *et al.*, Phys. Rev. Lett. **104**, 202501 (2010).
[6] C. Hartnack, H. Oeschler, and J. Aichelin, Phys. Rev. Lett. **96**, 012302 (2006).
[7] C. T. Sturm *et al.*, Phys. Rev. Lett. **86**, 39 (2001).
[8] B. Borderie and M. F. Rivet, Prog. Part. Nucl. Phys. **61**, 551 (2008).
[9] H. Stöcker *et al.*, Phys. Rev. Lett. **47**, 1807 (1981).
[10] A. Le Fèvre and J. Aichelin, Phys. Rev. Lett. **100**, 042701 (2008).
[11] W. Reisdorf *et al.*, Nucl. Phys. A **848**, 366 (2010).
[12] G. Lehaut *et al.*, Phys. Rev. Lett. **104**, 232701 (2010).
[13] J.-Y. Liu, W. J. Guo, S. J. Wang, W. Zuo, Q. Zhao, and Y. F. Yang, Phys. Rev. Lett. **86**, 975 (2001).
[14] X. G. Cao, G. Q. Zhang, X. Z. Cai, Y. G. Ma, W. Guo, J. G. Chen, W. D. Tian, D. Q. Fang, and H. W. Wang, Phys. Rev. C **81**, 061603(R) (2010).
[15] P. Danielewicz, B. Barker, and L. Shi, AIP Conf. Proc. **1128**, 104 (2009).
[16] T. Gaitanos, M. Colonna, M. Di Toro, and H. H. Wolter, Phys. Lett. B **595**, 209 (2004).
[17] W. Reisdorf *et al.*, Phys. Rev. Lett. **92**, 232301 (2004).
[18] Y. Zhang, Z. Li, and P. Danielewicz, Phys. Rev. C **75**, 034615 (2007).
[19] A. Andronic, J. Lukasik, W. Reisdorf, and W. Trautmann, Eur. Phys. J. A **30**, 31 (2006).
[20] S. Kumar, S. Kumar, and R. K. Puri, Phys. Rev. C **81**, 014601 (2010).
[21] J. Aichelin, Phys. Rep. **202**, 233 (1991).
[22] C. Hartnack, Rajeev K. Puri, J. Aichelin, J. Konopka, S. A. Bass, H. Stöcker, and W. Greiner, Eur. Phys. J. A **1**, 151 (1998).
[23] C. Hartnack, Li Zhuxia, L. Neise, G. Peilert, A. Rosenhauer, H. Sorge, J. Aichelin, H. Stöcker and W. Greiner, Nucl. Phys. A **495**, 303c (1989).
[24] J. Aichelin, A. Rosenhauer, G. Peilert, H. Stoecker, and W. Greiner, Phys. Rev. Lett. **58**, 1926 (1987).
[25] Y. G. Ma, R. Wada, K. Hagel, M. Murray, A. Ono, J. S. Wang, L. J. Qin, A. Makeev, P. Smith, and J. B. Natowitz, Phys. Rev. C **65**, 051602 (2002).
[26] Z. Chen *et al.*, Phys. Rev. C **81**, 064613 (2010).
[27] M. Huang *et al.*, Phys. Rev. C **81**, 044620 (2010).
[28] D. Lacroix, A. Van Lauwe, and D. Durand, Phys. Rev. C **69**, 054604 (2004).
[29] W. Müller, M. Begemann-Blaich, and J. Aichelin, Phys. Lett. B **298**, 27 (1993).
[30] K. Zbiri *et al.*, Phys. Rev. C **75**, 034612 (2007).
[31] Y. G. Ma *et al.*, Phys. Rev. C **71**, 054606 (2005).
[32] P. B. Gossiaux and J. Aichelin, Phys. Rev. C **56**, 2109 (1997).
[33] W. Reisdorf *et al.*, Nucl. Phys. A **612**, 493 (1997).